LEGAL NOTICE

This report was prepared by Ontario Hydro and, while effort has been made to assure the accuracy and applicability of the material contained herein, neither Ontario Hydro nor any person acting on its behalf:

(a) makes any warranty, express or implied with respect to the use of any information, apparatus, method or process disclosed in this report or that such use may not infringe privately owned rights; or

(b) assumes any liabilities with respect to the use of, or for damages resulting from the use of, any information, apparatus, method or process disclosed in this report.

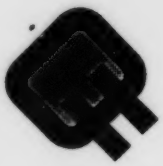

ontario hydro
research division

COMPLIMENTARY COPY
*Please Credit Ontario Hydro Research if Reproduced in Whole or in Part*

# Photoelectrochemical and Solid State Investigations of Sputtered Lead Oxide Films

*Report No 88-47-K*

L.C. Schumacher
Process Chemistry Section
Chemical Research Department

## *ABSTRACT*

Atomic sputtering has been employed to fabricate a new, thin (≤9000 Å) n-type semiconducting phase of lead oxide of approximate stoichiometry $PbO_{1.50}$. Films 1200 to 8800 Å in thickness deposited in a 100% $O_2$ plasma vacuum annealed 8 hrs reproducibly exhibited indirect bandgaps of ~1.18 eV, while films ~3200 Å and vacuum annealed ~ 1 hr displayed higher bandgaps of ~1.30 eV. Films deposited in a 50:50 mixture of $O_2$ and $N_2$ resulted in an oxide displaying a bandgap of ~1.44 eV. All films thicker than 4000 Å required vacuum annealing at ~250°C for periods of time > 2 hrs before any photoelectrochemical response was observed. The lower bandgap oxide phases are stable in aqueous alkaline media over a narrow potential range of ~0.20 V both in the dark as well as under chopped white light illumination (~200 mW/cm$^2$). These films have been characterized using a variety of techniques including XPS, Auger, X-ray diffraction, impedance and photoelectrochemical spectroscopies.



| job | file | date | report no. |
|---|---|---|---|
| 31-511-011 | 826.7 | February 10, 1989 | 88-47-K |

ontario hydro
research division

## EXECUTIVE SUMMARY

# Photoelectrochemical and Solid State Investigations of Sputtered Lead Oxide Films

*L.C. Schumacher*

Process Chemistry Section
Chemical Research Department

The development of economical $O_2$ electrode materials demonstrating both longevity and stability will in all likelihood be based upon a mixed oxide system. The challenge of designing such a material is considerable since two fundamental criteria must be satisfied. First, the material must reversibly incorporate $O_2$ in the vicinity of the thermodynamic $O_2$ redox potential. Secondly, the crystal lattice must be designed to facilitate rapid transport of oxide species through the lattice.

To maximize the chances for success in such an endeavour, a rapid, routine and reproducible method must be employed to fabricate the materials in a readily characterizable form. It is important that the measured electrocatalytic properties of the material so formed be minimally influenced by the method of fabrication. As well, the fabrication technique must be flexible enough to permit controlled variation of crystal composition and stoichiometry throughout the film. Atomic sputtering readily fulfills these conditions.

Atomic sputtering has been employed to fabricate a new, thin (≤9000 Å) n-type semiconducting phase of lead oxide of approximate stoichiometry $PbO_{1.50}$. Films 1200 to 8800 Å in thickness deposited in a 100% $O_2$ plasma vacuum annealed 8 hrs reproducibly exhibited indirect bandgaps of ~1.18 eV, while films ~3200 Å and vacuum annealed ~ 1 hr displayed higher bandgaps of ~1.30 eV. Films deposited in a 50:50 mixture of $O_2$ and $N_2$ resulted in an oxide displaying a bandgap of ~1.44 eV. All films thicker than 4000 Å required vacuum annealing at ~250°C for periods of time > 2 hrs before any photoelectrochemical response was observed. The lower bandgap oxide phases are stable in aqueous alkaline media over a narrow potential range of ~0.20 V both in the dark as well as under chopped white light illumination (~200 mW/cm$^2$). These films have been characterized using a variety of techniques including XPS, Auger, X-ray diffraction, impedance and photoelectrochemical spectroscopies.



| job | file | date | report no. |
|---|---|---|---|
| 31-511-011 | 836.7 | February 10, 1989 | 88-47-K |

## CONTENTS


| | | Page |
|---|---|---|
| 1. | INTRODUCTION | 1 |
| | 1.1 Electrocatalysis | 1 |
| | 1.2 Metal Oxides | 3 |
| | 1.3 Thin Films | 4 |
| | 1.4 Atomic Sputtering | 4 |
| | 1.5 Ex-Situ Studies | 6 |
| 2. | EXPERIMENTAL | 6 |
| | 2.1 Film Formation | 6 |
| | 2.2 Film Characterization | 7 |
| | 2.2.1 XPS Studies | 7 |
| | 2.2.2 Auger, IR and XRD Studies | 7 |
| | 2.2.3 Photoelectrochemical and Impedance Studies | 7 |
| 3. | RESULTS | 8 |
| | 3.1 Indium Tin Oxide Substrates | 8 |
| | 3.2 Lead Oxide | 8 |
| | 3.2.1 Solid State Properties | 8 |
| | 3.2.2 Photoelectrochemical Properties | 10 |
| 4. | DISCUSSION | 11 |
| 5. | CONCLUSIONS | 14 |
| 6. | ACKNOWLEDGEMENTS | 14 |
| 7. | SUGGESTIONS FOR FUTURE WORK | 15 |
| | REFERENCES | 16 |
| | FIGURES | 17 |
| | DISTRIBUTION | last page |

# LIST OF FIGURES


| Figure | |
|---|---|
| 1a | IR spectrum of lead oxide film deposited at 250°C and cooled immediately to room temperature. |
| 1b | IR spectrum of two lead oxide films deposited at ~250°C and vacuum annealed for 2 hrs (curve 1) and 8 hrs (curve 2). |
| 2a | Transmission spectra for $PbO_{1.5}$ films ~6400 Å thick grown on pyrex with different annealing times. |
| 2b | Transmission spectra for $PbO_{1.5}$ films ~6400 Å thick grown on quartz substrates with different annealing times. |
| 3 | XRD patterns for ~6400 Å lead oxide films grown on quartz illustrating the differences in crystal structure accompany differences in annealing times. |
| 4 | XRD patterns for ~6400 Å lead oxide all vacuum annealed 8 hrs showing the influence of substrate: a) pyrex; b) quartz; c) ITO; d) XRD pattern for the ITO substrate on pyrex. |
| 5 | Comparison of XRD spectra for 3000 Å and 64000 Å thick lead oxide films grown on ITO showing the presence of different phases as well as preferred orientation effects. |
| 6 | DC photocurrent decay in 0.10 M NaOH (curve 1) and 0.10 M KI and NaOH (curve 2). |
| 7 | Plot of photocurrent density versus lamp intensity. |
| 8 | AC quantum efficiency of ~6400 Å lead oxide film grown on ITO and vacuum annealed 8 hrs. |
| 9a | Indirect bandgap determination of ~6400 Å lead oxide film on ITO. |
| 9 | Indirect bandgap determination of ~3200 Å lead oxide film on ITO. |
| 10 | Photocurrent density at 570 nm measured against electrode potential showing slight hysteresis effect. |
| 11 | Mott-Schottky plots of lead oxide film (of Figure 8) measured in 0.5 M acetonitride giving $V_{fb}$ ~0.05 V (SCE). |

**Figure**


12 Mott-Schottky plots for lead oxide films all deposited at 250°C and: curve 1 - vacuum annealed 8 hrs; curve 2 - vacuum annealed 2 hrs; curve 3 - cooled to room temperature immediately.

13 Cyclic voltammogram showing that $Pb^{+2}$ is oxidized to $Pb^{+4}$ at 0.6 V (SCE) while $Pb^{+4}$ is reduced to $Pb^{+2}$ at -0.1 V (SCE).

14 Approximate energy level alignment of the vacuum annealed lead oxide film on ITO, based on experimentally measured $V_{fb}$ and $E_g$.

ontario hydro
research division

To: Dr. D. Mills
Director of Research

# Photoelectrochemical and Solid State Investigations of Sputtered Lead Oxide Films

## 1. INTRODUCTION

### 1.1. Electrocatalysis

Advances in the design and development of economical, efficient and stable electrocatalysts will have a significant impact in those energy intensive electrolytic industries where power costs are the dominant factor. Industries such as large scale water electrolysis and the chlor-alkali industry are two prime examples of such energy intensive industries. Conversely, power generation and storage processes utilized in systems such as fuel cells and storage batteries would also benefit significantly from improved electrocatalysts. The rate of energy consumption (generation) by an electrochemical cell is given by IV, where I is the cell current and V the cell voltage, which may be expressed by

$$| V - \Delta E_e | = IR + \eta_a + \eta_c + \eta_{ca} + \eta_{cc}$$

where $\Delta E_e$ is the difference between the equilibrium or reversible potentials for the anodic and cathodic reactions, IR the ohmic losses incurred by all current carrying elements in the cell, and $\eta_a$ and $\eta_c$ are the activation overpotentials associated with the interfacial anodic and cathodic electrode reactions respectively while $\eta_{ca}$ and $\eta_{cc}$ are the concentration overpotentials for the anodic and cathodic reactions (1). The greater the irreversible contributions, $IR + \eta_a + \eta_c + \eta_{ca} + \eta_{cc}$, the greater the energy consumption (less the energy production) of the cell and hence the lower the efficiency. The minimization of both the IR drop and concentration overpotentials is essentially an engineering problem associated with optimum cell design.

The activation overpotentials can be represented by the Tafel relation; $\eta = \frac{2.3\,RT}{\alpha\, n\, F} \log (I/I_o)$ where F is the Faraday, n the number of electrons transfered, R the gas constant, T the temperature, $\alpha$ the transfer coefficient and $I_o$ the exchange current density. An electrode

| job | file | date | report no. |
|---|---|---|---|
| 31-511-011 | 836.7 | February 10, 1989 | 88-47-K |

exhibiting a low overpotential at practical current densities must be characterized by a high exchange current density, $I_o$, while a low Tafel slope, 2.3 RT/$\alpha$ nF is determined by the mechanism of the interfacial reaction. The goal of designing efficient electrocatalysts is achieved principally through maximizing the exchange current density, though different catalysts can also result in different mechanisms and hence different Tafel slopes.

In several of the applications mentioned above, fuel cells, certain battery systems and the chlor-alkali industry, the cathodic reaction of choice is the overall oxygen reduction half cell reaction,

$$O_2 + 4H^+ + 4e^- = 2H_2O\,, \quad E_{o_2/H_2o} = 1.23\ eV\,.$$

The design and fabrication of a practicable $O_2$ reduction electrodes remains one of the challenging problems in the field of electrocatalysis. Exchange current densities of the order of $\sim 10^{-10} - 10^{-11}$ amps - $cm^{-2}$ are ~7 orders of magnitude smaller than for the $H_2$ oxidation electrode. There are essentially two pathways by which the oxygen reduction reaction can proceed, the 2 and 4 electron pathway

$$\begin{array}{l} \qquad\qquad\quad (+4H^+ + 4e^-) \longrightarrow H_2O \\ \Big\lceil \\ O_2 \\ \Big\lfloor \\ \qquad\quad (+2H^+ + 2e^-) \longrightarrow H_2O_2 \; -(+2H^+ + 2e^-) \longrightarrow 2H_2O \end{array}$$

The desired pathway is the 4 electron route since it is more energy efficient in the absence of overpotentials for the first step of the 2 electron processes. As well, the peroxide generated by the $2e^-$ pathway chemically attacks carbon which is the catalyst support usually used, with the result being disintegration of the electrode. The choice of cathode materials for oxygen reduction is a materials science problem in that the catalyst must be designed in order that the strong $O_2$ bond can be easily ruptured at some point in the reaction. This is why the transition metals and metal oxides are being studied and developed as potential oxygen electrodes. In general, adsorption of the reactant molecule on the electrode depends on the number of unpaired d-electron and empty d-orbitals which are able to form bonds with the adsorbate. Since the free energy of adsorption will depend on the number of unpaired electrons per atom and also on their energy levels, it follows that by changing both by alloying or other means one can change the free energy of adsorption. For the case of very weak adsorption (low heat of adsorption) a low rate of bond dissociation results giving rise to low exchange current densities, while for the case of too strong adsorption, oxidation of the electrode will occur, also decreasing the exchange current density for the desired reaction. Consequently the maximum oxygen reduction rate will occur at intermediate values of the free energy of adsorption, ie. for a material which sits atop the "volcano plot" of exchange current density versus free energy of adsorption for a series of oxygen cathode materials.

## 1.2. Metal Oxides

The main categories of oxygen cathode materials which have been identified are: *1) the active and noble metals, 2) transition metal based oxides*, and *3) organometallic complexes (metal macrocyles) all supported on high surface area carbons.*

Our efforts at fabricating and screening potential oxygen cathode materials is centered in part around the mixed metal oxides. There are several fundamental reasons for this course of action. First, most of the noble metals are unstable with respect to their oxides in the vicinity of the reversible oxygen potential. Even gold has a monolayer of oxide on its surface under $O_2$ evolution conditions. Therefore, the class of catalysts referred to above as noble metals really refers to oxide coated noble metals. Secondly, greatly enhanced electrocatalytic activity and stability of the carbon supported metal macrocycles is achieved by high temperature (~800 - 900°C) annealing in an inert atmosphere (2). The results of the surface analysis of the products of this treatment indicate the presence of both nitrogen coordinated metals and metal oxides, specifically cobalt and iron, hence again the metal oxides are implicated. Finally, many oxides have been shown to perform as peroxide elimination catalysts in the two electron reduction of $O_2$ (1). Therefore, it is clear that the metal oxides are playing a major role in $O_2$ electroctalysis.

Recent research in the search for a practicable $O_2$ electrode has centred in part around mixed oxides such as spinels, pyrochlores and perovskites, the interest in these materials being based in large part upon the fact that they exhibit conductivities orders of magnitude higher than most simple oxides. This arises due to the presence of cations in more than one valence state in the lattice. Our interest in the spinels, perovskites and pyrochlores, is based in part on the above as well as the fact that these materials can exist over a wide range of stoichiometry and composition. This is an important consideration in designing an oxygen electrode since we feel it is almost inevitable that oxygen uptake by the electrode will be one of the steps in the reaction, and this in turn will be determined by the ability of the lattice to reversibly incorporate oxygen in the potential region near the reversible oxygen potential.

The focus of this preliminary study has been to assess atomic sputtering as a method of fabricating metal oxide materials to be screened as $O_2$ reduction catalysts. The goal of this study has been to characterize reactively sputtered lead oxide films. The choice of lead oxide is based on the fact that the lead ruthenium pyrochlores, $Pb_2 [Ru_{2-x} Pb_x] O_{7-y}$ where $0 \leq x \leq 1$ and $0 \leq y \leq 0.5$, have previously been reported as exhibiting reversible behaviour as an $O_2$ electrode in the bulk form (3). Therefore, it is reasonable to assume that a lead-ruthenium oxide of the same stoichiometry in the thin film form should exhibit significant activity as an $O_2$ electrode. In fact, other mixed metal pyrochlores have displayed considerable electrocatalytic activity in the bulk form, hence a comprehensive screening of these materials in the thin film form is indicated. However, before meaningful results can be obtained with the mixed metal compounds, an understanding of the properties of the sputtered Pb and Ru oxides separately should be obtained first. The fabrication and characterization of reactivity sputtered lead oxide films has been undertaken with the goal of ascertaining: 1) the effect on the solid state properties of fabrication conditions such as substrate temperature and post formation annealing procedures; 2) the impact of substrate material on the crystal

structure; 3) the predominant valence state(s) for metal species which can exist in more than one oxidation state; and 4) the presence of any thickness effects.

### 1.3. Thin Films

These studies are restricted to thin films $10-10^4$ Å in thickness for several reasons. First, most metal oxides are semiconductors and consequently the low conductivities will result in increased ohmic losses thereby reducing the electrocatalytic activity. Secondly, a fundamental question remains as to the role of the crystal structure in determining the electrocatalytic properties of a material. It should be possible to fabricate by sputtering thin films with the same stoichiometry as the corresponding bulk forms but different in structure from the bulk crystal. Comparison of the electrocatalytic activity of these thin films with published data on the bulk forms will give qualitative information regarding the impact of crystal structure on electrocatalytic behaviour. Further, the as formed thin films can be subsequently annealed at high temperatures in an attempt to induce crystallization into that of the bulk crystal structure. Comparison of the electrocatalytic properties of the resulting structures to the as formed films will also shed light on the importance of crystal structure on electrocatalytic behaviour. Similarly, the possibility exists for observing new or normally metastable phases in the thin film form. For example, in very thin films the substrate may have a significant influence on the crystal structure, particulary when the film is grown layer by layer, so that epitaxial growth becomes possible. Also, in thin films higher crystal energies can occur since factors such as surface tension will be more pronounced, thereby resulting in potentially new crystal phases.

### 1.4. Atomic Sputtering

Atomic sputtering is a physical vapour deposition technique. The target and substrates are in a vacuum chamber held at ~10 microns chamber pressure. The gas, which can be inert eg. argon, is ionized, thereby creating a glow discharge from which positively charged ions are accelerated to the cathode or target material, held at a negative potential. Collision of these high energy ions with the target results, through momentum transfer, in the ejection of atoms from the latter. These sputtered atoms then condense onto a substrate suitably placed with respect to the target. Sputter deposition in an inert gas will result in films of approximately the same composition as the target material, while sputtering in the presence of a reactive gas such as oxygen, can result in the formation of an oxide film.

There are several unique advantages associated with atomic sputtering as a film growth technique which are worthy of exploitation. Since the deposition technique involves momentum transfer, any material, liquid or solid, can be sputter deposited. This is particularly advantageous for growth of refractory materials with high melting points which cannot be easily evaporated. Substantial control over film adhesion properties is another advantage associated with atomic sputtering. Depending on sputtering gas pressure, the kinetic energy of the ejected target atoms can be an order of magnitude greater than the mean energy of thermally evaporated atoms (4). This higher kinetic energy can result in intermixing of the sputtered atoms with the substrate material, thereby leading to better

adhesion. Further, in multitarget sputtering systems, it is possible to form graded junctions with two or more materials of any desired thickness and composition, thus giving one flexibility in reducing thermal expansion and lattice mismatch, an important consideration in applications such as high temperature solid oxide fuel cells. Significant control over film composition is also possible with sputtering. Not only can target materials of any composition be employed, but with multitarget deposition systems one can simultaneously deposit from two or more targets. By variation of the biasing potential on each target and the substrate table rotation speed, films covering the full composition range can be made.

Atomic sputtering with appropriate deposition conditions usually leads to smooth films. This is desirable when characterization of the catalytic material is the goal. While high surface areas are required in a practical working electrode system, they prevent elucidation of the true electrocatalytic activity of the material. The inability of determining the inherent electrocatalytic activity properties of dispersed metal oxides is to date one of the major stumbling blocks to gaining a proper understanding of those properties which are necessary for achieving good electrocataytic activity. Comparison of materials fabricated by different techniques will in general result in substantially different microgeometries, thereby rendering comparisons of performance very difficult.

While atomically homogeneous films can be produced by sputtering, it is also possible to produce films with controlled concentration gradients throughout the film. The latter are likely to exhibit electronic and electrocatalytic properties different from the former, thereby resulting perhaps in new electrocatalytic materials.

A further complication can arise from impurity incorporation into the oxide, which will also be dependant on the fabrication procedure. For example, the inclusion of chloride or nitrates into films grown by the decomposition of liquid chlorides or nitrates respectively results in oxides exhibiting different electrocatalytic behaviour (5). Since atomic sputtering is a physical vapour deposition technique and oxygen is both the sputtering gas and a reactant, it will be possible to eliminate such uncontrolled impurities.

The composition of the sputtering gas is also a major consideration in determining the composition of the sputtered film. Argon is used when the desired film composition is that of the target material. Films sputtered in the presence of reactive gases (eg. $O_2$,$H_2$,$N_2$) will result in general in the incorporation of these materials into the film structure. In this way oxides, hydrides, nitrides and mixtures of these can be fabricated from a metallic target. Alternatively, one can employ an oxide or ceramic target initially and use argon as the sputtering gas to produce oxide films. However, there are several disadvantages to this approach. Ceramic targets tend to be porous and hence will trap impurity gases which can contaminate the films. Also, insulating ceramic targets cannot be deposited using DC sputtering, due to charging problems. Variation of the reactive gas composition, for example $Ar/O_2$, will result in oxide films of varying M/O ratios (M = metal). Furthermore, if a lattice can take up nitrogen, variation of the ratio of two reactive gases $O_2/N_2$ can result in films characterized by an anion sublattice with a varying O/N composition. This will result in a different environment for the *d* electrons and since it is the *d* electrons which are responsible for the strength of interaction between the reactant molecule and the electrode, by fine tuning

the *d* levels, one is fine tuning the electrocatalytic properties of the material. There are very few fabrication techniques where this type of control over lattice composition is possible.

### 1.5. Ex-situ Studies

Historically, a major limitation in the study of electrocatalyst systems has been a lack of detailed molecular level knowledge at the of the electrode surface. Since even submonolayer surface layers can drastically alter the electronic properties of a surface, it is important that ex-situ techniques such as photoelectron spectroscopy (XPS), Auger electron spectroscopy and secondary ionization mass spectroscopy (SIMS) be exploited in characterizing the surface and bulk properties of electrocatalysts. A particularly important application of ex-situ studies is for identifying the oxidation state(s) of the cation species at the surface and in the bulk of the film. This is essential for identifying the electrocatalytically active or important species in the oxide matrix. One major disadvantage of the Auger and XPS techniques is that they cannot be used to quantitatively discriminate between different valence states of a given metal species in the bulk, this being due to reduction of the cations during sputter profiling. However, a combination of IR and Raman spectroscopy can be employed to qualitatively identify bulk species in various oxidation states.

## 2. EXPERIMENTAL

### 2.1. Film Formation

All films were grown by atomic sputtering using a Perkin-Elmer model 2400 rf diode sputtering system. A substrate heater table allows maximum substrate temperatures in the range 350-400°C to be achieved. Thickness calibrations were obtained by weighing and assuming bulk densities for the sputtered films. All films were grown on pyrex microscope slides which had been ultrasonically cleaned in 2-propanol followed by degreasing in 2-propanol vapour and then heated in vacuo to ~250°C for 3-4 hours before deposition commenced. For photoelectrochemical and electrocatalytic studies indium tin oxide (ITO) was used as the conducting back contact, these films being deposited from a $In_2O_3$ 10%$SnO_2$, 6" diameter ceramic target to a thickness of ~4 x $10^3$Å. The lead oxide films were fabricated using a 6" diameter lead metal target obtained from Materials Research Corp. (MRC); 99.99% pure. The oxide films were formed by reactive sputtering in a 100% $O_2$ plasma at a chamber pressure of 10 microns at substrate temperatures ranging from room temperature to 250°C. Previous studies have shown that depositing the oxide in a mixed $Ar/O_2$ plasma results in films with inferior solid state properties compared to those formed in a 100% $O_2$ plasma (6). Following film deposition, if no annealing was planned, the substrates were cooled to room temperature over 3 hrs and the samples removed. If an annealing program was planned, the substrate heater was adjusted to the appropriate temperature and the films annealed for periods of time up to 12 hrs.

## 2.2. Film Characterization

### 2.2.1. XPS Studies

X-ray photoelectron spectroscopy and Raman studies were carried out using the facilities of Surface Science Western at the University of Western Ontario.

### 2.2.2. Auger, IR and XRD Studies

X-ray diffraction and Auger depth profile studies were performed by the Analytical Department at Ontario Hydro Research Division. Infrared spectra of films deposited onto silicon substrates were obtained using a Nicolet 1040 FTIR spectrometer.

### 2.2.3. Photoelectrochemical and Impedance Studies

Characterization of the semiconductor properties of the metal oxides was accomplished using photoelectrochemical and impedance techniques. Wavelength dependent action spectra were recorded using a Spex Minimate monochromator and a 150 W zenon lamp. Action spectra were recorded either by direct illumination of the electrode and measurement of the resulting DC photocurrent, or chopped illumination and the measurement of the AC photocurrent using a phase sensitive amplifier. The AC technique is the preferred one when characterizing semidconductors which suffer from poor kinetics for charge transfer at the interface. In the DC method, the measured photocurrent is the current crossing the semiconductor electrolyte interface. In the AC technique, since the electrode is capacitively coupled, the quantity measured is not simply the current crossing the semiconductor-electrolyte interface. Thus, the AC technique permits the characterization of those semiconductors which exhibit a transient DC photoresponse arising from poor charge transfer kinetics. AC quantum efficiencies were calculated using the expression $\Phi_{AC} = 1.2408\ J/I_o\lambda$, where J is the photocurrent density ($\mu A - cm^{-2}$), 1.2408 is conversion factor relating photon flux density to power flux density and $I_o$ is the incident power flux density ($mW - cm^{-2}$) at wavelength $\lambda$ (nm). The photoelectrochemically determined bandgaps were obtained by plotting $(\Phi_{AC}h\upsilon)^{1/2}$ vs $h\upsilon$ where h is Planck's constant and $\upsilon$ the photon frequency. Such a plot will be linear with the intercept on the energy axis yielding the band-gap, $E_g$, for those semiconductors where $E_g$ arises from an indirect optical transition (7).

Impedance properties of the films were measured using a phase sensitive amplifier and signal generator. By modelling the space charge region as a capacitance in series with a resistance and measuring the in- and out- of phase components of the current, the space charge capacitance can be calculated. The expression relating the space charge capacitance, C, to the solid state properties is given by $C^{-2} = \frac{2}{K\varepsilon_o q N_d}\ (V - V_{fb})$ where K is the relative dielectric constant, $\varepsilon_o$ the permittivity of free space, q the charge on the proton, $N_d$ the doping density of the semiconductor, V the applied potential and $V_{fb}$ the flatband potential, the potential which must be applied so that the energy bands are flat up to the surface of the semiconductor

(8). According to this equation, a plot of $C^{-2}$ versus V will be linear with the potential intercept yielding $V_{fb}$ and the slope inversely proportional to the doping density, $N_d$.

## 3. RESULTS

### 3.1. Indium Tin Oxide Substrates

The choice of substrate material is important for studies of the electrocatalytic properties of thin films. The possibility of the substrate in influencing the crystal structure of the film has been mentioned already. In addition to this, the substrate will have an impact on the electronic properties of the film. First, the metal oxide films must make ohmic contact with the underlying substrate as failure to achieve this will result in increased overpotentials, the source of this being the non-ohmic nature of the film-substrate interface.

It is also desirable that the substrate exhibit a high overpotential for the electrode reaction of interest to ensure that it makes no contribution to the electrode process. This is particularly important when films of <100 Å are under investigation where tunneling effects become important.

Finally, the substrate should not be capable of being oxidized under $O_2$ reduction conditions as electrochemical oxidation of the substrate could obscure the reaction under study. The material chosen as the conducting substrate, indium tin oxide (ITO) has been tested and shown to exhibit high overpotentials for both oxygen evolution and reduction. It is a degenerate n-type semiconductor and expected to make ohmic contact to most of the wide bandgap semiconducting oxides. ITO is highly stable in aqueous media for pH > 6.0. The conductivity of these films, as measured by a two probe technique, was of the order of $\sim 10^4\ \Omega^{-1}\ -cm^{-1}$ and therefore, at low current densities should serve very well as a conducting substrate.

### 3.2. Lead Oxide

#### 3.2.1. Solid State properties

The results of XPS studies of reactively sputtered films of lead oxide deposited both at room temperature and at 250°C and cooled immediately to room temperature showed the presence of three species of lead, $Pb^0$, $Pb^{+2}$ and $Pb^{+4}$. These films were highly conductive, this being attributed to the presence of elemental lead. Compositional analysis of these films indicated that the different species of lead were present as $Pb^0$ ~45%, $Pb^{+2}$ ~30% and $Pb^{+4}$ ~18%. The oxygen spectrum reveals that of the oxygen species present, 45% is lattice oxgen while the remaining 55% correspond to different species of oxygen, either as hydroxide or molecular oxygen.

Films vacuum annealed for 8 hrs at 250°C contained only two species of lead, $Pb^{+2}$ and $Pb^{+4}$. These films were ~8 orders of magnitude more resistive than the films cooled immediately to

room temperature. Compositional analysis reveal that the two lead species are present in the amount $Pb^{+2}$ ~56% and $Pb^{+4}$ ~41%. Of the oxygen species present, ~85% is lattice oxygen while ~15% corresponds to other species, such as hydroxide or molecular oxygen. Further in-situ vacuum annealing of these films for ~30 min at 260°C did not produce any significant change in the overall oxygen to lead ratio.

The results of Auger depth profile studies indicate a relatively constant O/Pb ratio of ~1.50 is maintained throughout the vacuum annealed film. Due to reduction of lead species during the sputter depth profile, it was not possible to observe any variation in the $Pb^{+2}/Pb^{+4}$ ratio throughout the film. There is, however, general agreement between the XPS and Auger studies that the films vacuum annealed for 8 hrs contain both $Pb^{+2}$ and $Pb^{+4}$ and that the overall O/Pb ratio is ~1.50.

The far infrared spectra of three sputtered lead oxide films, all deposited on silicon substrates are shown in Fig. 1. The film deposited at 250°C and cooled immediately to room temperature is featureless, see Fig. 1a. In Fig. 1b a film deposited at 250°C and vacuum annealed for two hrs (curve 1) is compared to a film of identical thickness but vacuum annealed 8 hrs (curve 2). The transmission spectra for the films vacuum annealed for 2 and 8 hrs but deposited on quartz and pyrex are displayed in Fig. 2. Note that these films were formed at the same time as the films on silicon, hence they were fabricated under identical conditions, except for substrate material. The IR spectrum of the vacuum annealed films do not correspond to those previously reported for $\alpha$-$PbO_2$, PbO and $Pb_3O_4$ (9).

X-ray diffraction (XRD) studies of lead oxide deposited on various substrates and with various post formation treatments are displayed in Fig. 3, 4 and 5. The XRD spectra for films on quartz (~6400 Å in thickness) and vacuum annealed for 2 and 8 hrs (Fig. 3) show significant differences. The almost complete disappearance of diffraction lines at 26°, 36° and 53° for the film annealed 8 hrs compared to that annealed 2 hrs suggests a change in crystal phase occurs during the vacuum annealing process. Note also the significant change in relative peak intensities for the two films. While the appearance or disappearance of peaks will result from changes in crystal structure, changes in relative peak intensities can be indicative of changes in crystal orientation. Comparison of the XRD spectrum for the film annealed 8 hrs with catalogued lead oxide suggest the possible presence of the $PbO_{1.57}$ phase in addition to an uncatalogued phase(s).

The influence of substrate material on the crystal structure is illustrated in Fig. 4. Spectra 1, 2 and 3 are for the same thickness of lead oxide deposited and vacuum annealed (8 hrs) at 250°C. The only difference is substrate material with the film of curve 1 grown on pyrex, that of curve 2 on quartz while curve 3 is for a film grown on ~4000 Å ITO which is on a pyrex flate. Curve 4 of Fig. 4 is the XRD spectrum for such an ITO film grown on pyrex, ~4000 Å in thickness. While there are major phase changes even going from pyrex to quartz substrates, the most substantial phase change occurs in films grown on ITO, (compare curve 3 to 1 and 2). The almost complete disappearance of the diffraction peaks centered at 23.5°, 48° and 49° indicate major phase changes while the substantial change in relative peak intensities suggest substrate orientation affects.

In addition to annealing time and substrate material, film thickness is also a factor influencing the crystal structure of these lead oxide films. Figure 5 compares the XRD spectra for two films of thickness ~6400 Å and 3000 Å, grown on ITO substrates. From this it can be seen that different phases are present in addition to preferred orientation affects on going from 3000 to 6400 Å.

### 3.2.2. Photoelectrochemical Properties

Films sputter deposited at room temperature onto ITO exhibited no photoresponse, either AC or DC. Similarly, films sputtered at 250°C and cooled immediately to room temperature displayed no detectable AC or DC photoresponse. However, films fabricated and vacuum annealed at ~250°C for periods of time ranging from ~1 to 8 hrs displayed substantial AC and DC photoanodic behaviour. The DC photoanodic response was transient in nature with a slow decay observed. Curve 1 of Fig. 6 shows this behaviour for a 6400 Å thick film under monochromatic illumination in $N_2$ purged 0.10 M NaOH. Curve 2 of Fig. 6 is the transient decay of this same electrode, but in a solution of .1 M KI in 0.10 M NaOH. Using the AC technique to measure the photoresponse gave stable and reproducible photoanodic behaviour. A plot of AC photocurrent density versus light intensity for monochromatic illumination is essentially linear, Fig. 7. On the other hand, under much higher intensity white light illumination (~200 mW–cm$^2$), a photocurrent versus light intensity plot is highly non-linear. An electrode illuminated for 3 days under ~200 mW–cm$^{-2}$ white light intensity displayed no detectable photocorrosion or photodegradation under +0.22 V (SCE). Furthermore, no significant change in either bandgap or doping density occurred after this period of time.

The AC quantum efficiency for a ~6400 Å thick lead oxide film (vacuum annealed 8 hrs) shown in Fig. 8 displays a photocurrent onset in the vicinity of 1000 nm (1.18 eV). An indirect bandgap determination for the 6400 Å thick film, obtained by plotting $(\Phi h\upsilon)^{1/2}$ vs $h\upsilon$, yields an indirect bandgap of $E_g$ ~1.18 eV, see Fig. 9a. A similar plot for the 3200 Å thick film, shown in Fig. 9b, extrapolates to $E_g$ ~1.30 eV, also indirect.

The photocurrent behaviour at 570 nm shows a slight hysteresis effect for potential scanning to potentials anodic of 0.30 V (SCE), see Fig.10. Scanning to more positive potentials resulted in irreversible degradation of the photoresponse. Similarly, potential scanning in the region negative of 0.0 V (SCE) also resulted in irreversible degradation of the film. Stable and reproducible photoanodic behaviour was obtained only in the narrow potential region between 0.10 V to 0.30 V (SCE) in 0.10 M NaOH.

Since the electrode could only be scanned over a narrow potential range, 0.20 V, without irreversible changes to the solid state properties, it was not possible to obtain meaningful impedance data in aqueous media. Therefore, in order to measure the impedance properties of these films, a nonaqueous solvent was employed. Specifically, acetonitile was employed as the solvent with sodium perchlorate as the supporting electrolyte at a concentration of 0.5 M. The Mott-Schottky plots corresponding to the electrode of Fig. 8 are displayed in Fig.11 at four frequencies. As can be seen, these plots are linear over a 0.7 V range, all extrapolating to give $V_{fb}$~0.05 V (SCE), while yielding doping densities in the range 1 x 10$^{18}$ cm$^{-3}$ at 2 x 10$^3$ Hz to 3.4 x 10$^{18}$ at 10$^2$ Hz, assuming a dielectric constant of 26 (10).

Figure 12 compares the Mott-Schottky behaviour at $10^3$ Hz for three different electrodes all deposited for the same length of time and substrate temperature (250°C), but with different post formation annealing times. Curve 1 is for the film vacuum annealed for ~8 hrs, curve 2 for the film vacuum annealed for ~2 hrs and curve 3 for a film cooled to room temperature immediately after formation. The steady decrease in doping density accompanying the increase in annealing time was reproducible. The far infrared spectra of an identical set of films deposited at the same time but on silicon are shown in Fig. 1.

As pointed out above, applying bias potentials greater than 0.30 V versus flat band in aqueeous media and negative of flat band resulted in irreversible changes to the film properties. The oxidation peak centered at +0.6 V (see Fig. 13) versus flat band arises due to $Pb^{+2}$ being oxidized to $Pb^{+4}$ while the broad reduction peak centered at -0.10 V versus flat band is due to $Pb^{+4}$ being reduced to $Pb^{+2}$ (11). Potential switching between -0.10 V and 1.10 V (both versus flat band) result in these films displaying an electrochromic effect, where at -0.10 V the films are transparent while at 1.10 V they are dark. Based on the fact that this behaviour was observed in aqueous media only, it was concluded that $OH^-$ species is involved in the process, similar to electrochromic effects displayed by other noble metal based oxides such as iridium oxide (12). Switching between -0.10 V and 1.10 V (SCE) continuously for ~24 hrs resulted in irreversible degradation of the films.

## 4. DISCUSSION

The lead oxide films formed both at room temperature and 250°C followed by immediate cooling to room temperature are a composite of elemental lead and various lead oxides, $\alpha$–$PbO_2$ and PbO. The XRD results suggest that these films are highly disordered. Considering that oxygen is in exess during sputter deposition, the presence of elemental lead is taken as evidence that at least some of the sputtered species are lead atoms. A yellowish film on the lead target indicates the presence of orthorhombic PbO on the target surface. The effect of post formation annealing conditions, film thickness and choice of substrate material is having a very pronounced impact on the solid state properties of these films.

The effect of varying the vacuum annealing time at 250°C from 2 to 8 hrs on the crystal structure, photoelectrochemical and impedance properties can be understood in part as follows. Films formed at 250°C initially contain three species of lead, $Pb^0$, $Pb^{+2}$ and $Pb^{+4}$ and a substantial amount of nonlattice oxygen. Upon vacuum annealing, the elemental lead oxidizes to either $Pb^{+2}$ or $Pb^{+4}$. As the ratio of $Pb^{+4}/Pb^{+2}$ increases from ~.60 prior to vacuum annealing to ~1 after, this suggests that the elemental lead is oxidizing to both $Pb^{+2}$ and $Pb^{+4}$. The data indicates that most of the elemental lead is oxidized within 2 hrs of vacuum annealing at 250°C, this based on the film conductivities and XPS results. However, further vacuum annealing up to 8 hrs is still resulting in major crystal phase changes. This further change must be examined in light of the relative ionic radii of $Pb^{+4}$ (0.84 Å) $Pb^{+4}$ (1.20 Å) and $O^{-2}$ (1.26 Å), these being based on the set reported by Shannon and Prewitt (13).

In those metal oxides where the $M^{+z}$ ionic radius is much smaller than the $O^{-2}$ radius (.6 to 1.0 Å compared to 1.26 Å) the oxide ions form a close packed lattice with both tetrahedral and octahedral holes, which are then filled by the $M^{+z}$ cations. When the cation can exist in

more than one oxidation state, where again both cation radii are much less than the oxide ion radii, then the same situation exists as above, the only difference being that the distribution of cations in the tetrahedral and octahedral holes will be determined in part by the ratio of the cation radii. On the other hand, when one of the cation species is close to or comparable in size to the oxide ion, as is the case with $Pb^{+2}$, the crystal packing arrangement is not so straightforward. The perovskites are characterized by the formula $ABO_3$ where $A^{+2}$ is of roughly the same diameter as the oxide ion $O^{-2}$ and $B^{+4}$ is much smaller. Therefore, $A^{+2}$ and $O^{-2}$ determine the crystal structure with the much smaller $B^{+4}$ being distributed among the available holes. Both XRD and IR data suggest that films vacuum annealed 8 hrs are crystallized into perovskite structure. As evidence by the IR results, there is a continuous change from a disordered lattice to a sprectrum with five well defined bands accompanying increased annealing time. Such a spectrum is characteristic of oxides exhibiting the perovskite structure (14).

The Mott-Schottky plots of Fig. 12 reveal a decrease in doping density, $N_d$, accompanies increased vacuum annealing time. The film conductivity also decreased with annealing time. These observations appear to be at variance with what might be expected since these lead oxide films would be expected to be n-type semiconductors by virtue of either lead excess or oxygen deficiency. Since vacuum annealing is having the effect of reducing the as formed lead oxide down to a phase with a stoichiometry near $PbO_{1.50}$, one might expect an increase in conductivity and doping density to occur. It appears the lead oxide is transforming to a low conductivity phase.

The effect of film thickness on the photoelectrochemical properties is also quite pronounced. Comparison of the XRD patterns for a 3200 Å and 6400 Å thick lead oxide films on ITO reveal the presence of two different phases for these two thicknesses, a result further supported by the two photoelectrochemically determined bandgaps. For the 3200 Å thick film $E_g$ ~1.30 eV while for 6400 Å film $E_g$ ~1.18 eV. Both bandgaps are indirect (see Fig. 9) as would be expected for an oxide where the optical transition is usually from the $O_{2p}$ based valence band to the metal based 6s or 6p conduction band. These bandgaps are substantially lower than those previously reported for any phase of lead oxide, $\alpha$–$PbO_2$ (~1.40 eV), PbO(~2.73 eV) and $Pb_3O_4$(~2.12 eV), (15). The fact that the lowest bandgap is much less than that of $\alpha$–$PbO_2$ and PbO indicates that this oxide cannot be considered a solid solution of these two oxides. If it were, then by Vergard's rule one would expect the bandgap to take on a value intermediate between that of $\alpha$–$PbO_2$ and PbO (14). It should be pointed out that the lowest bandgap measured for the thick films (~1.18 eV) in the studies, while being the lowest reported to date, may not represent the lowest existing for lead oxide. Consider the case of tetragonal (red) versus rhombehedral (yellow) PbO with the former exhibiting a bandgap of ~2.0 eV compared to 2.8 eV for the latter. Tetragonal PbO is structurally different from the rhombehedral form in that the divalent lead cation is asymmetrically coordinated to its light nearest neighbors, this distortion being attributed to the "inert pair effect" (14) where the 6 $s^2$ electron pair are in fact located in a hybridized s-p orbital and therefore not spherically symmetric. Similarly, in a perovskite structure with both $Pb^{+4}$ and $Pb^{+2}$ present, such distortions may also exist, resulting in structures displaying different energy gaps. Consequently, 1.18 eV may not represent the minimum bandgap obtainable with the lead oxide system.

Comparison of these photoelectrochemically determined bandgaps with the optical transmission spectra of these same films, compare Fig. 2 and 9, indicate the former is a far more reliable method of obtaining energy gaps compared than the latter. The stability of these films in 0.10 M NaOH under ~200 mW-cm$^{-2}$ white light illumination for ~3 days (the length of the experiment) with no evidence of photocorrosion at 0.20 V overpotential with respect to flat band indicates that this material may have potential photovoltaic application. While the AC quantum efficiencies in the vicinity of 600 nm (the maximum in the solar spectrum) are low, 10-15% (see Fig. 8), it should be pointed out that this system is far from optimized for maximum quantum efficiency. Figure 13 shows the energy level alignment of the lower energy gap lead oxide phase in relation to the levels of the conducting ITO substrate and the $OH^-/O_2$ redox couple in aqueous media. This alignment is based on the experimentally determined flat band potential, $V_{fb}$ , and $E_g$ for this phase of $PbO_{1.50}$in conjunction with the known solid state properties of ITO (16). From this alignment it can be seen that there is considerable energy mismatch between the conduction bands of ITO and $PbO_{1.50}$ which could result in a non-ohmic junction. This would result in a barrier to electron flow from the $PbO_{1.50}$ to the ITO, giving rise to a loss in quantum efficiency. Non-linear i-V curves from conductivity measurements through the $PbO_{1.50}$ / ITO films as well as non-linear photocurrent versus light intensity (at high intensities) observed for these films are taken as supporting evidence for the presence of this non-ohmic junction. Consider also that the conduction band edge of $PbO_{1.50}$ is ~.25 eV above the $OH^-/O_2$ redox level. This means that once a bias potential ≥.25 eV is applied to the electrode, the conduction band will drop below the $OH^-/O_2$ redox level which will then allow tunneling of electrons from the conduction band back to the surface which will result in the reduction of any species oxidized by the photogenerated holes in the valence band. This will result in a loss of photocurrent for anodic potentials greater than 0.32 V versus flat band. The presence of surface states will act as recombination centres which will also reduce the quantum efficiency. Evidence for the existence of surface states comes from the frequency dispersion in the Mott-Schottky plots of Fig. 8, such behaviour being normally attributed to surface states. The decay in the DC photocurrent with time (Fig. 6) is also indicative of surface states. A slower DC photocurrent decay was observed when KI was present in solution where the $I^-$ may be interacting with the surface to tie up recombination centres. The low DC photocurrents observed with these films are probably due to the non-ohmic back contact as well as the fact that only a narrow space charge region could be established because of the limited potential range in which this phase is stable. The optimum energy alignment at both the conducting substrate and the oxide-electrolyte interface which would be required for obtaining maximum quantum efficiencies is illustrated in Fig. 14.

The irreversible loss of photoanodic response attendant with applied anodic potentials >0.30 V versus flat band is most likely due to an increase in lattice defect density as $Pb^{+2}$ is oxidized to $Pb^{+4}$. Also, since $Pb^{+2}$ is oxidized to $Pb^{+4}$ the lattice is expected to undergo a phase change, similar to that observed for various vacuum annealing conditions, due to a variation in the relative concentration of the $Pb^{+2}$ and $Pb^{+4}$ species. This explains why the stable phase formed by 8 hrs vacuum annealing of the sputtered films is electrochemically (and photoanoidcally) stable only over a narrow potential region of ~0.30 V.

On the other hand it is interesting to note that those metal oxides which display both longevity and reversible electrochromism contain metal cations in two or more oxidation states but which have similar ionic radii. For example, in the tungsten bronzes the two predominant cations of tungsten, $W^{+6}$ (0.62 A) and $W^{+4}$ (0.70 A) are within 10% of each other (13).

## 5. CONCLUSIONS

It has been shown that a new and stable, thin film crystalline phase of lead oxide with a stoichiometry of $Pb_2O_3$ can be prepared by atomic sputtering. This highly crystalline phase exhibits a bandgap of $E_g$ ~1.18 eV which is substantially lower than that reported for the other phases of lead oxide. Vacuum annealing at temperatures in the vicinity of ~250°C of the sputtered films is a prerequisite of obtaining this low bandgap phase as well as photoconductivity. The stability of this material over a 0.7 V range in non-aqueous media coupled with the demonstrated photostability under high intensity white light illumination suggest that this phase of lead oxide may have possible photovoltaic applications in the thin film form.

## 6. ACKNOWLEDGEMENTS

The author would like to thank Professor Michael Dignam and the University of Toronto for unlimited use of the atomic sputtering apparatus. Thanks are due to Mr. Ingo Holzhueter for performing some of the electrochemical studies and to Mr. Brian Pattendon for the X-ray studies. Support in the form of an Industrial Research Fellowship from the Government of Canada is gratefully acknolweged.

## 7. SUGGESTIONS FOR FUTURE WORK

(1) One of the goals of this investigation, stated at the outset, was to assess the viability of atomic sputter deposition as a fabrication method for producing new materials to be screened as $O_2$ electrodes. The new low bandgap phase of lead oxide produced in this study clearly shows the utility of atomic sputtering as a means of producing new materials. Based in part on these results it appears that full exploitation of sputtering in the fabrication of binary and ternary alloy and oxide materials should be vigorously pursued at this time. The fact that different crystal structures can be obtained with the mixed oxides depending on synthesis conditions of pressure and temperature suggests that in addition to sputtering, the same composition materials should be fabricated under high pressure conditions and the solid state and electrocatalytic properties compared to those of the sputtered films.

Approved by:

D.J.R. Dodd
Manager
Chemical Research Department

Prepared by:

L.C. Schumacher
Chemist
Process Chemistry Section

Reviewed by:

S.H. Hawthorne
Unit Head
Process Development

## REFERENCES


(1) D. Pletcher, Electrocatalysis: Present and Future, J. Appl. Electrochem., 14 , 403 (1984.

(2) E. Yeager, J. Electrochem. Soc., 128 , 160C, (1981).

(3) H.S. Horowitz, J.M. Longo, and H.H. Horowitz, Oxygen Electrocatalysis on Some Oxide Pyrochlores, J. Electrochem. Soc., 130 , 1851 (1983).

(4) W.D. Westwood, Glow Discharge Sputtering, Progress in Surface Science 7 , (1976).

(5) S. Trasatti, Electrochemica Acta, 29 , 1503 (1984).

(6) M.F. Weber, L.C. Schumacher and M.J. Digman, J. Electrochem. Soc., 129 , 2022 (1982).

(7) M.A. Butler and D.S. Ginley, "Semiconductor Liquid Junction Solar Cells", ed. A. Heller. The Electrochemical Society Softbound Proceedings Series, Princeton, N.J., 1977.

(8) N.F. Mott, Proc. Roy. Soc. (London), A171 , 27 (1939).

(9) N.T. McDevitt and W.L. Baun, Spectrochemica Acta, 20 , 799 (1964).

(10) G.V. Samsonov, The Oxide Handbook, Plenum Publishing Corp., 1973.

(11) R. Yue, C.G. Chen and S.F. Xie, Extended Abstracts, J. Electrochem. Soc., Fall Meeting, 2016 (1987).

(12) S. Hackwood, G. Beni, W.C. Dautremont-Smith, L.M. Schiavone and J.L. Shay, Appl. Phys. Lett., 37 , 965 (1980).

(13) R.D. Shannon and C.T. Prewitt, Acta Cryst., B 26 , 1046 (1970).

(14) A.R. West, Solid State Chemistry and Its Applications, John Wiley & Sons Ltd.

(15) W.H. Strehlow and E.L. Cook, J. Phys. Chem. Ref. Data, 2 , 163 (1973.

(16) E.Y. Wang and L. Hsu, J. Electrochem. Soc., 125 , 1328 (1978).

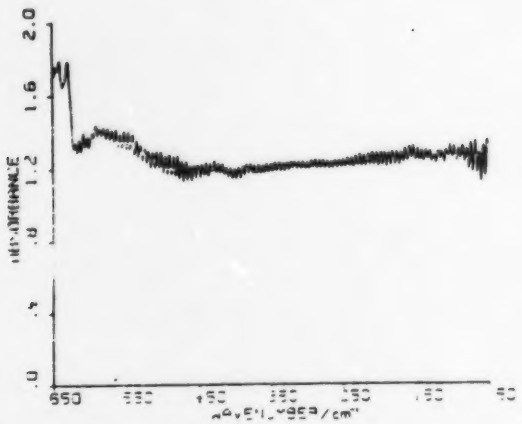

Figure 1a: IR spectrum of lead oxide film deposited at 250°C and cooled immediately to room temperature.

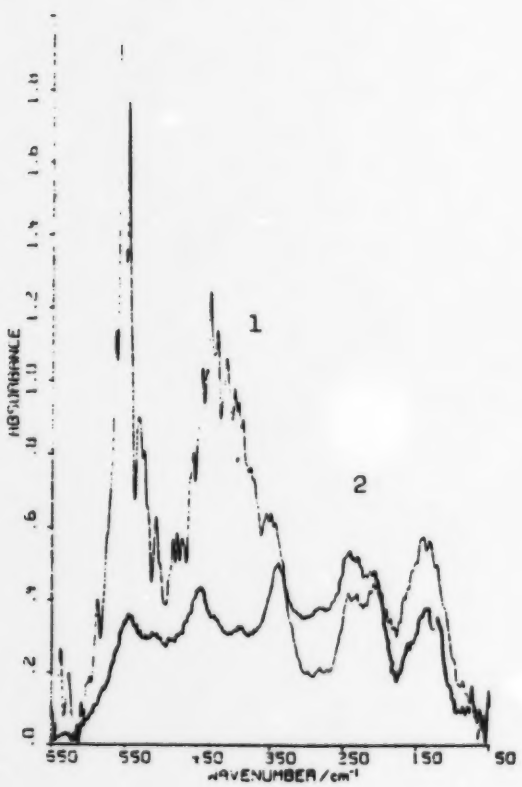


Figure 1b: IR spectrum of two lead oxide films deposited at ~250°C and vacuum annealed for 2 hrs (curve 1) and 8 hrs (curve 2).

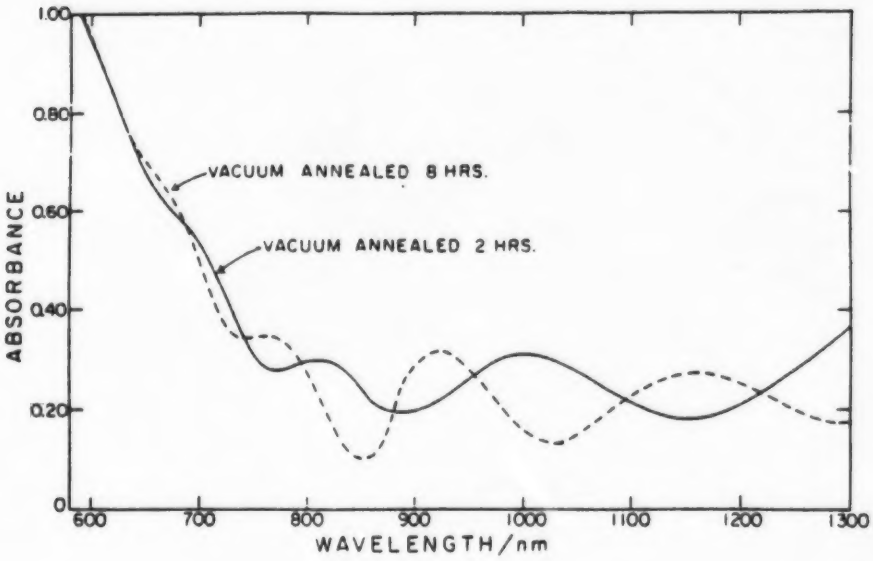


Figure 2a: Transmission spectra for $PbO_{1.5}$ films ~6400 Å thick grown on pyrex with different annealing times.

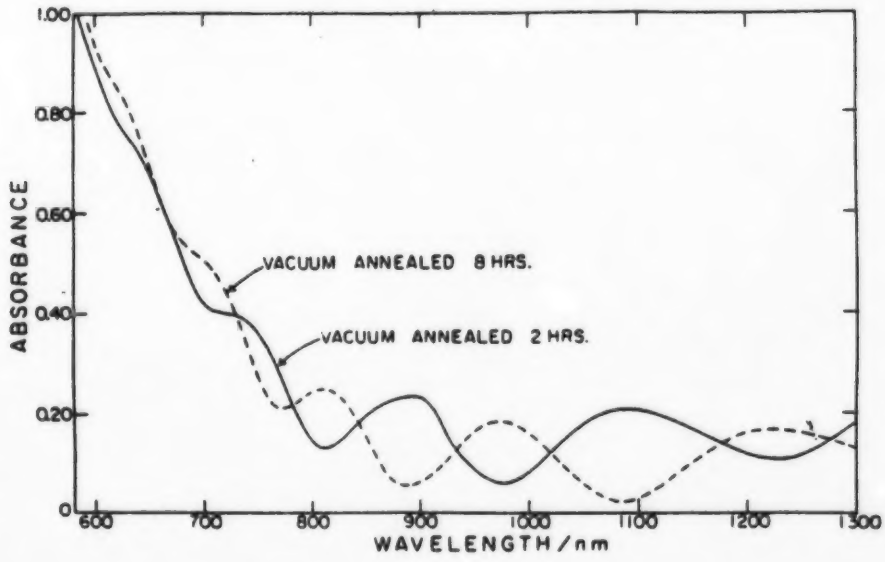


Figure 2b: Transmission spectra for $PbO_{1.5}$ films ~6400 Å thick grown on quartz substrates with different annealing times.

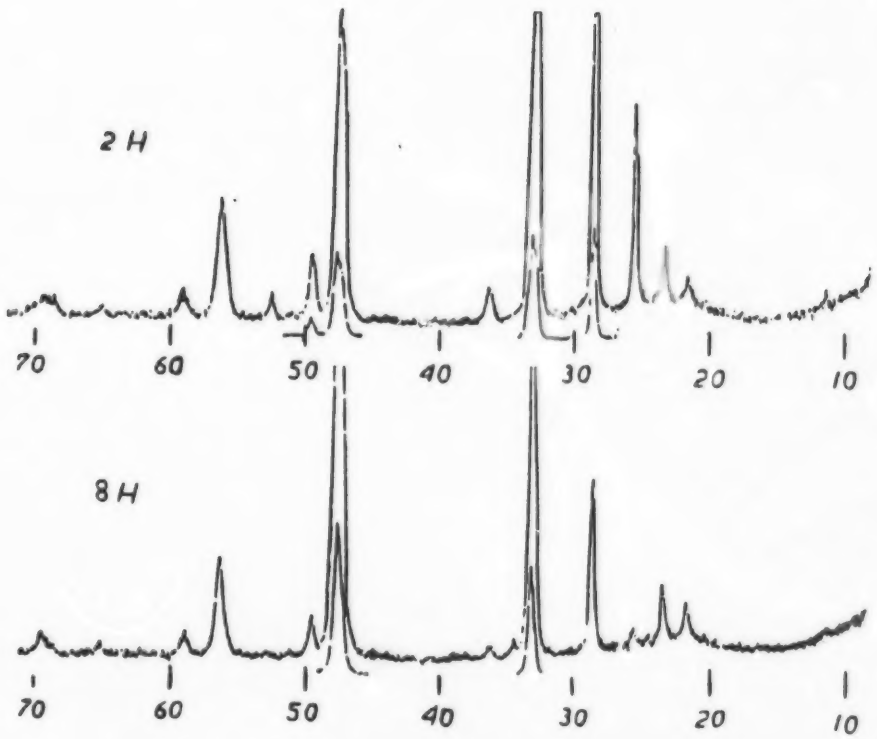


Figure 3: XRD patterns for ~6400 Å lead oxide films grown on quartz illustrating the differences in crystal structure accompany differences in annealing times.

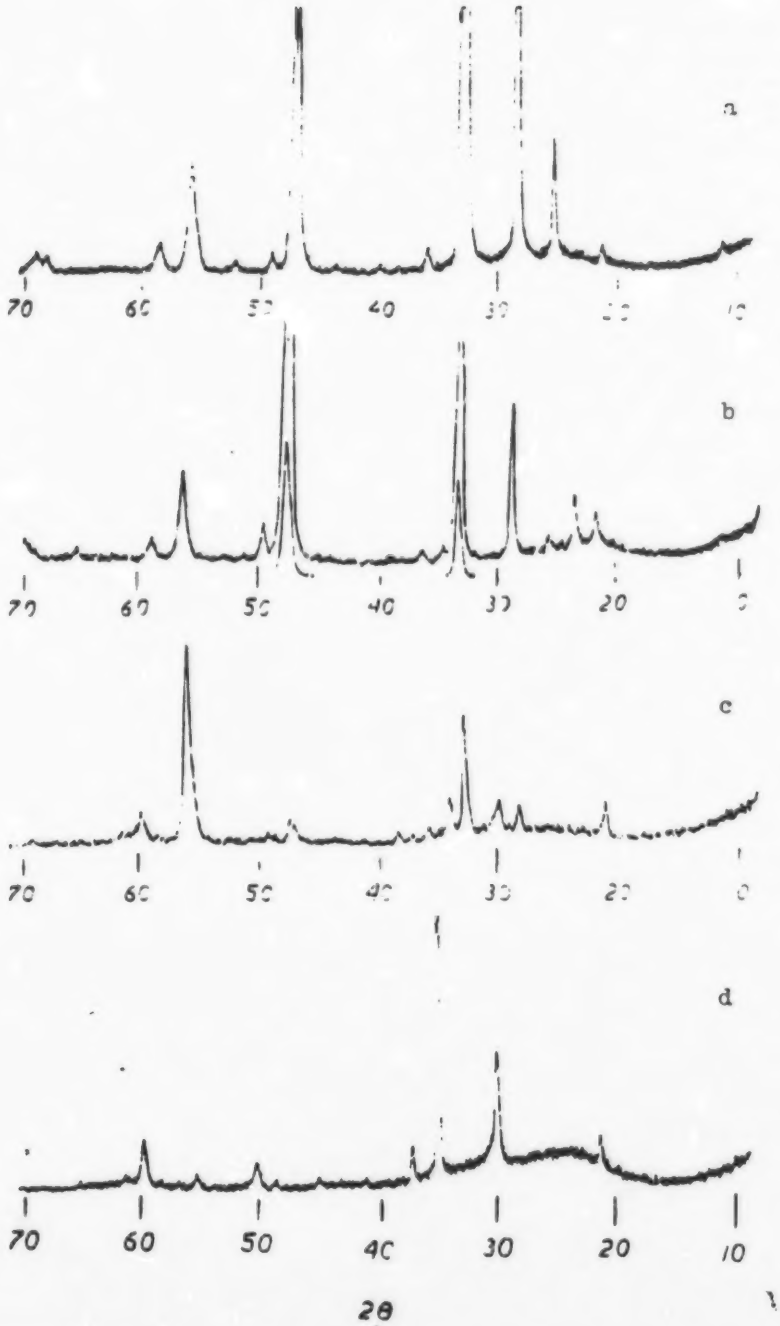


Figure 4: XRD patterns for ~6400 Å lead oxide all vacuum annealed 8 hrs showing the influence of substrate: a) pyrex; b) quartz; c) ITO; d) XRD pattern for the ITO substrate on pyrex.

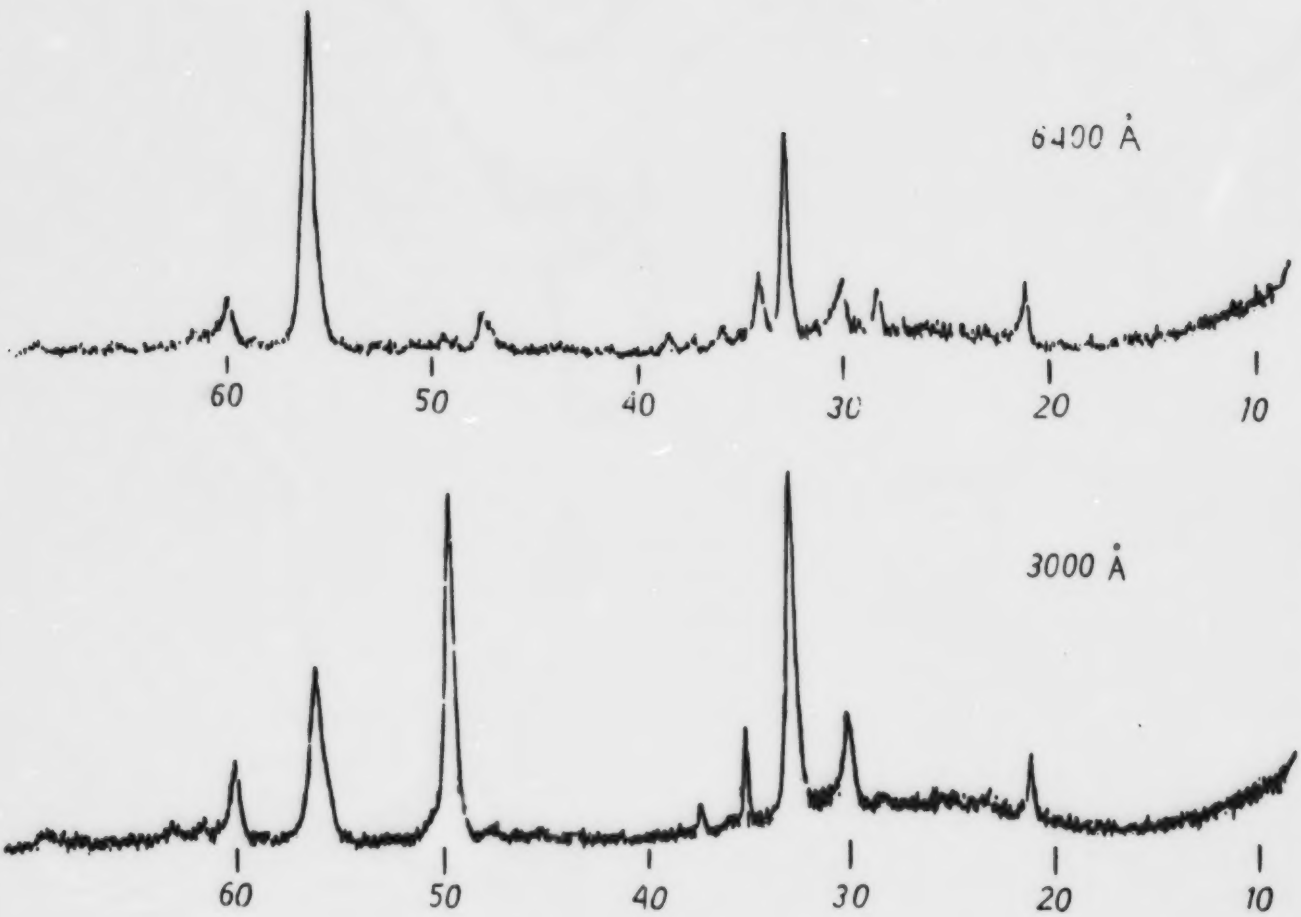


**Figure 5:** Comparison of XRD spectra for 3000 Å and 64000 Å thick lead oxide films grown on ITO showing the presence of different phases as well as preferred orientation effects.

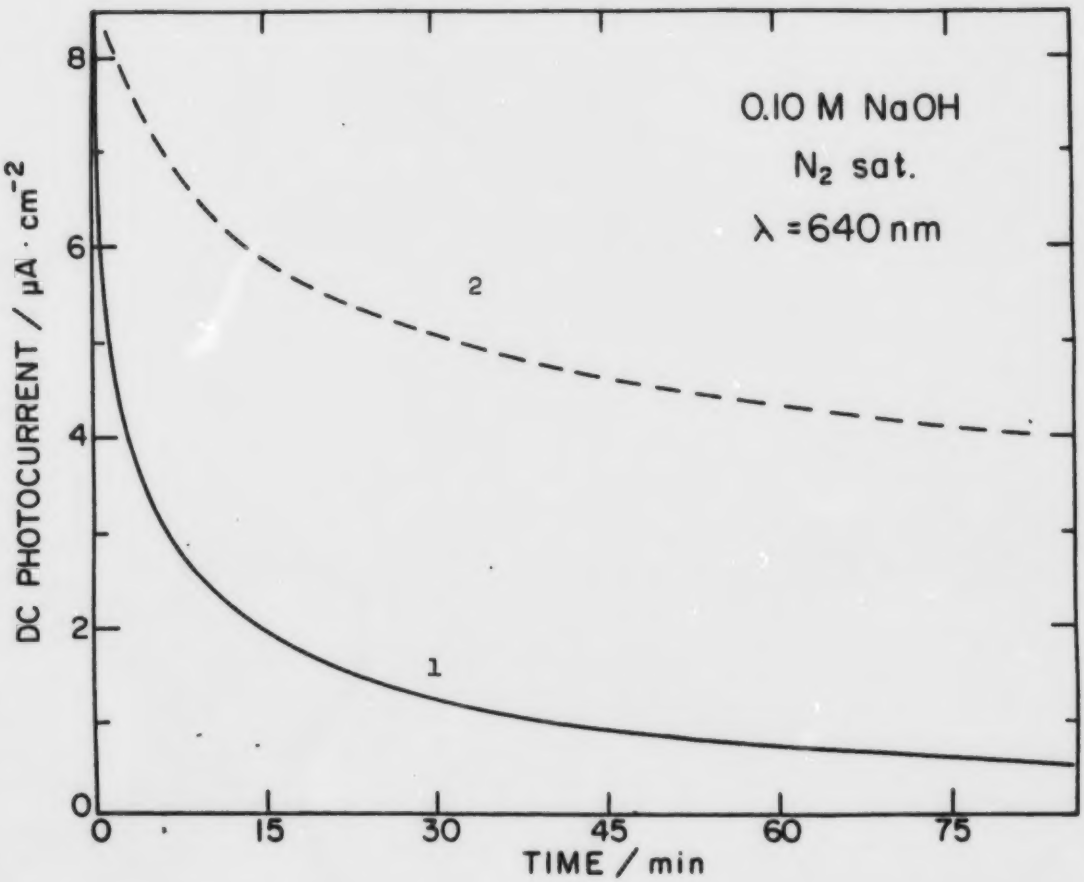


Figure 6: DC photocurrent decay in 0.10 M NaOH (curve 1) and 0.10 M KI and NaOH (curve 2).

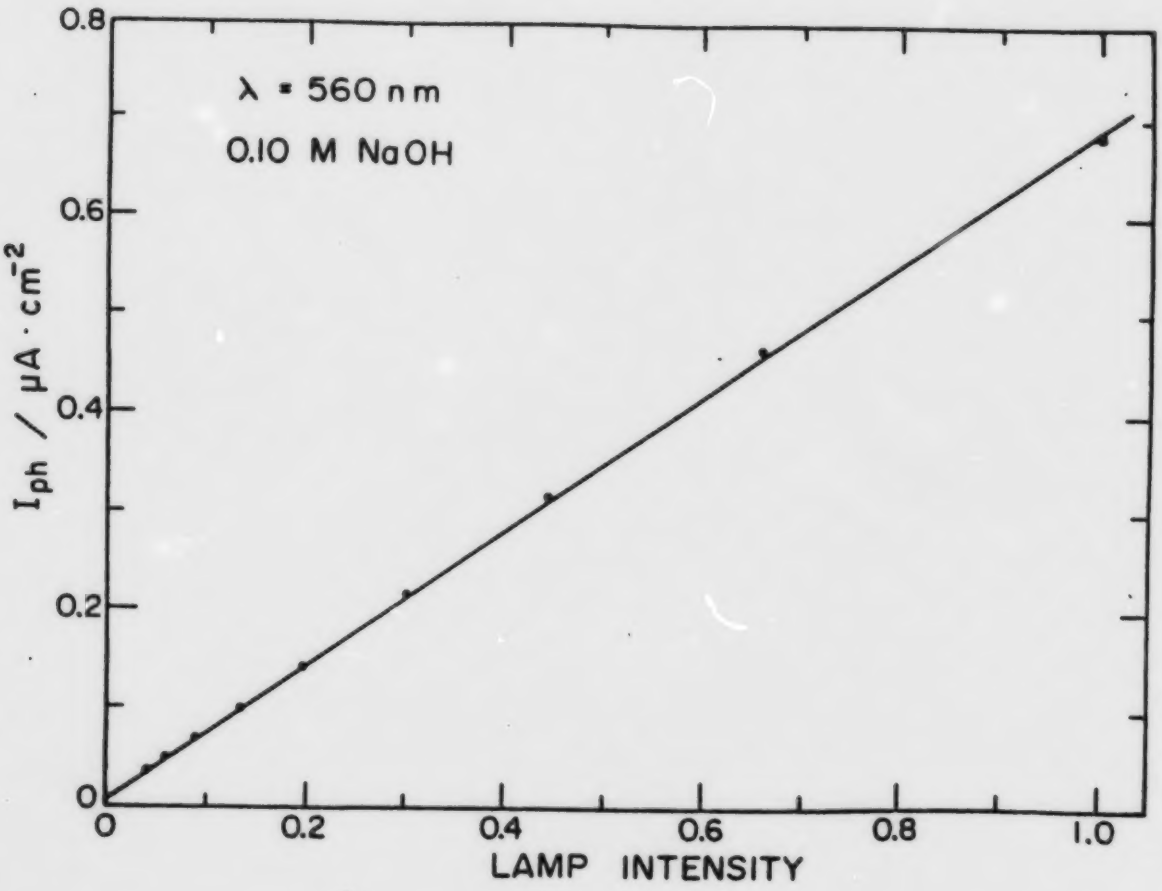


Figure 7: Plot of photocurrent density versus lamp intensity.

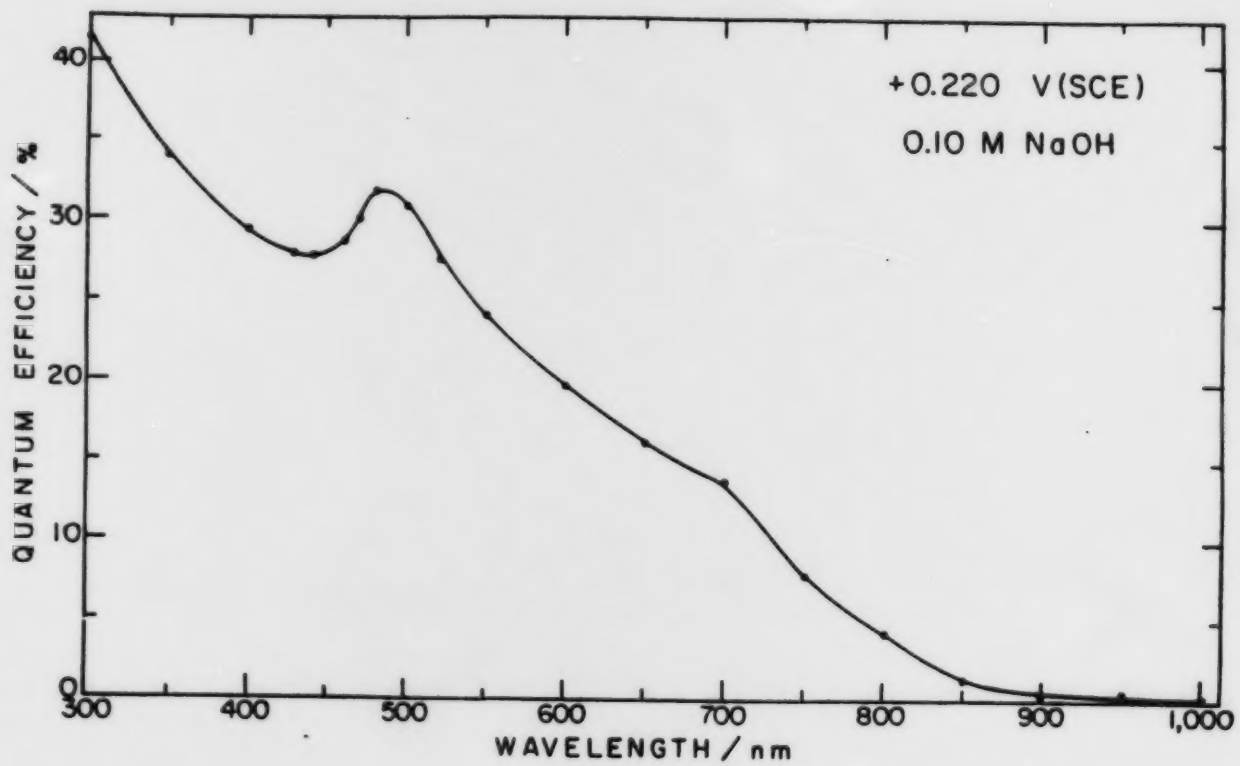


**Figure 8:** **AC quantum efficiency of ~6400 Å lead oxide film grown on ITO and vacuum annealed 8 hrs.**

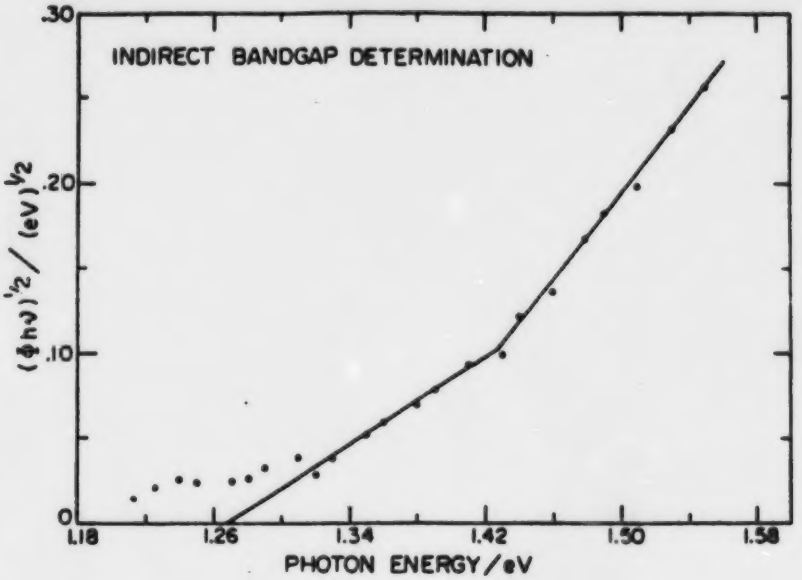


Figure 9a: Indirect bandgap determination of ~6400 Å lead oxide film on ITO.

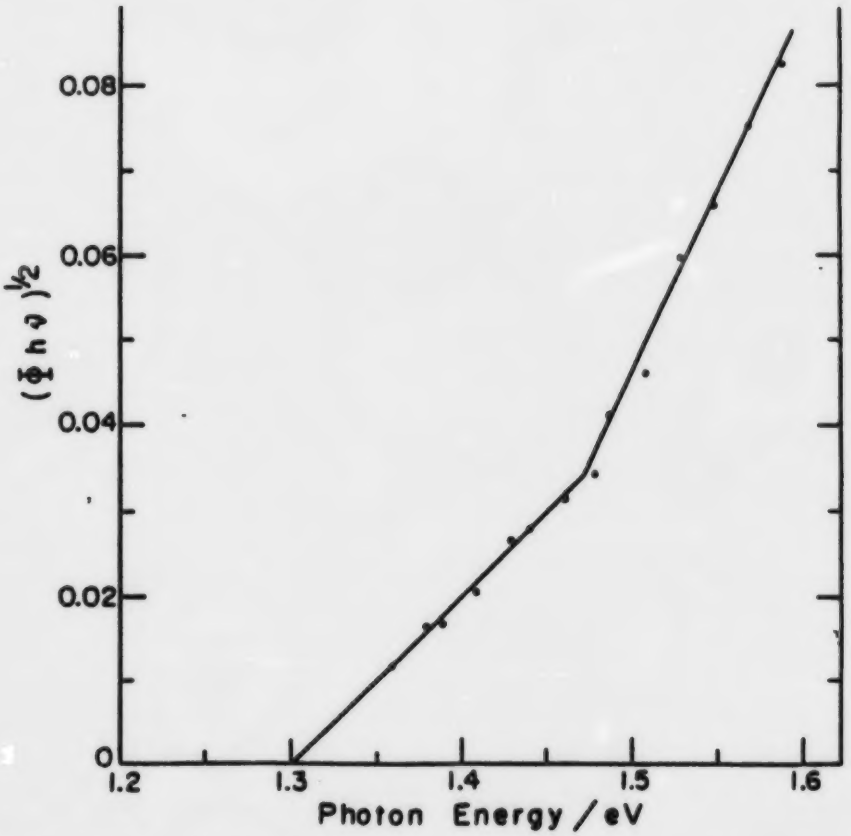


Figure 9b: Indirect bandgap determination of ~3000 Å lead oxide film on ITO.

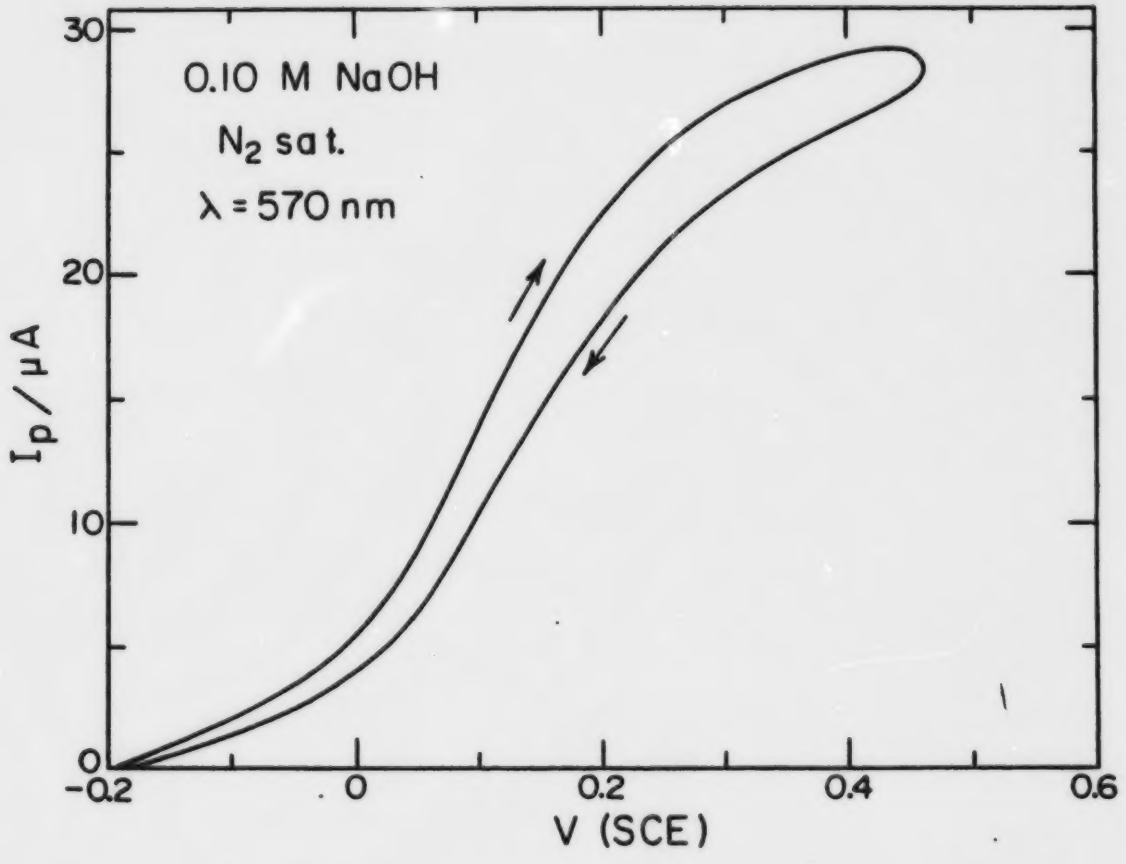


Figure 10: Photocurrent density at 570 nm measured against electrode potential showing slight hysteresis effect.

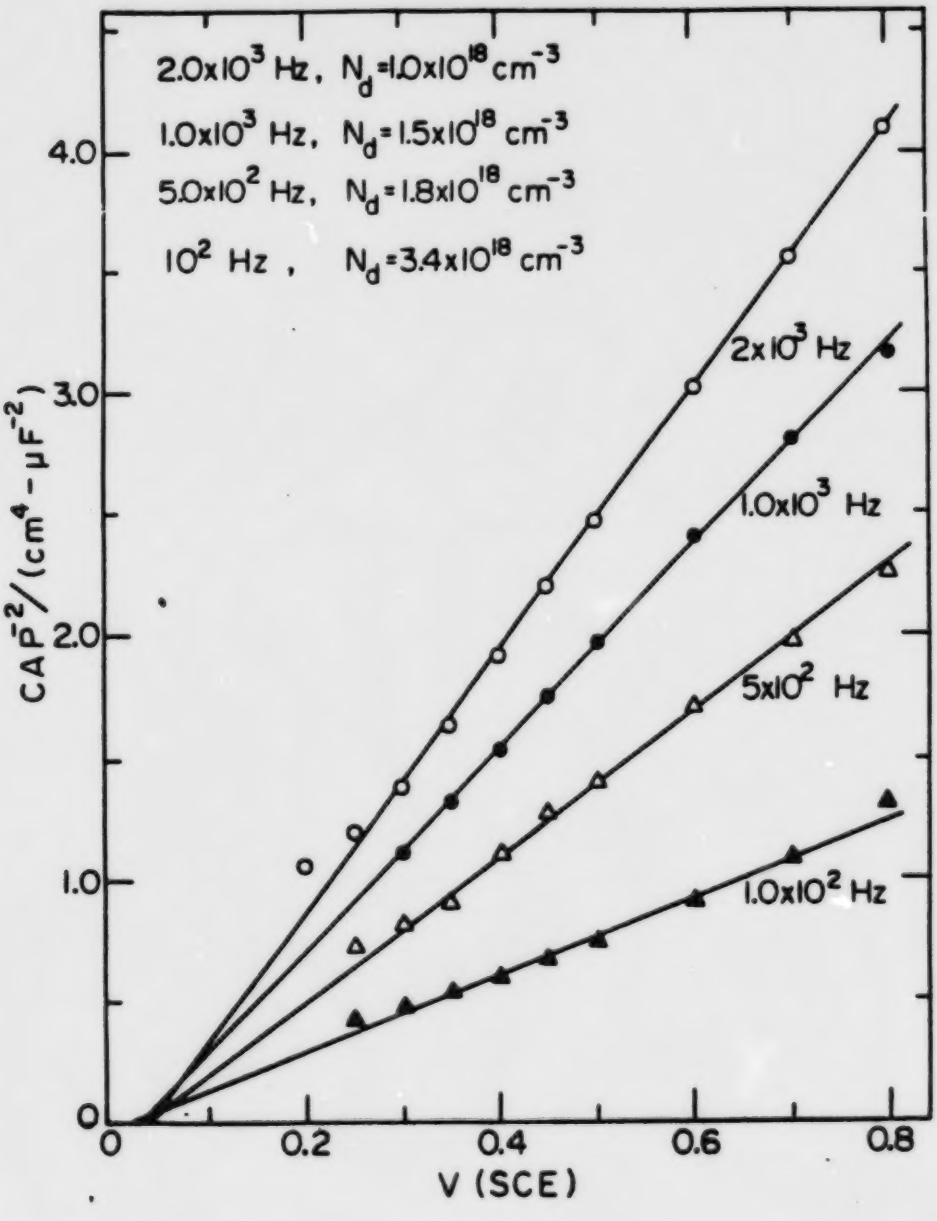


**Figure 11:** Mott-Schottky plots of lead oxide film (of Figure 8) measured in 0.5 M acetonitride giving $V_{fb}$ -0.05 V (SCE).

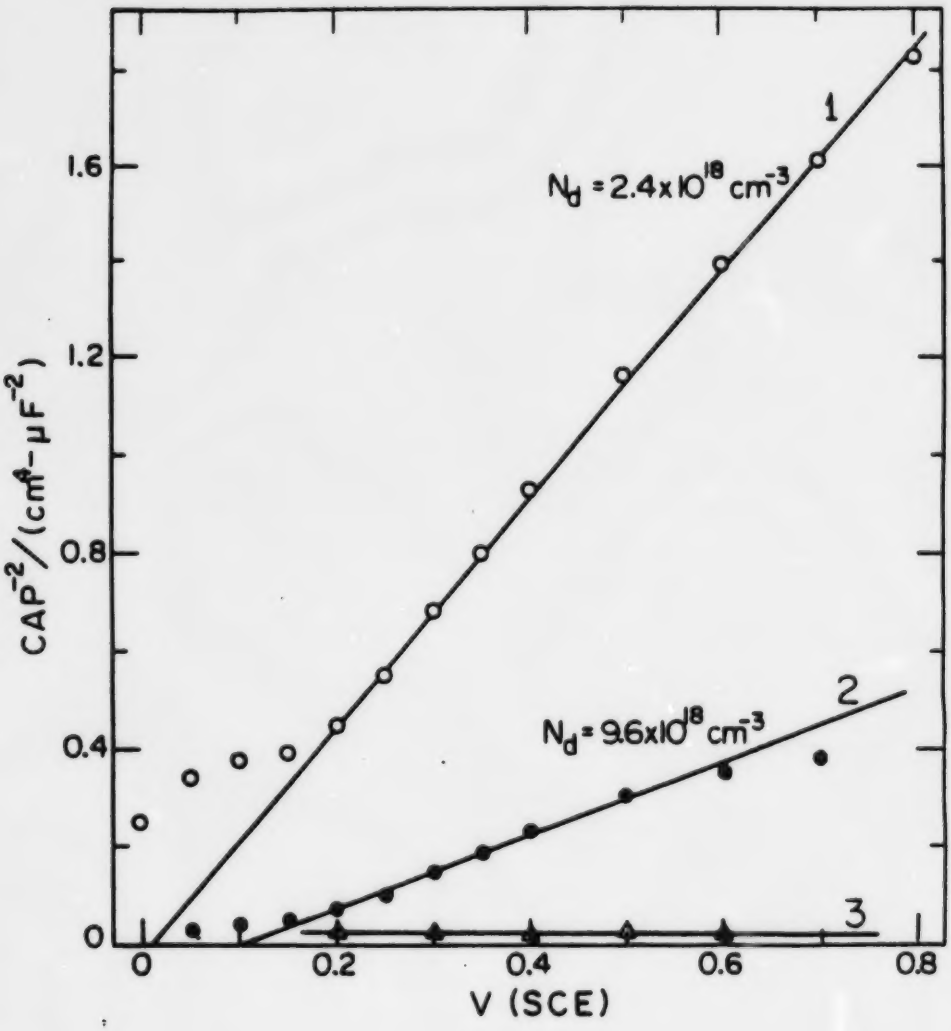


**Figure 12:** Mott-Schottky plots for lead oxide films all deposited at 250°C and: curve 1 - vacuum annealed 8 hrs; curve 2 - vacuum annealed 2 hrs; curve 3 - cooled to room temperature immediately.

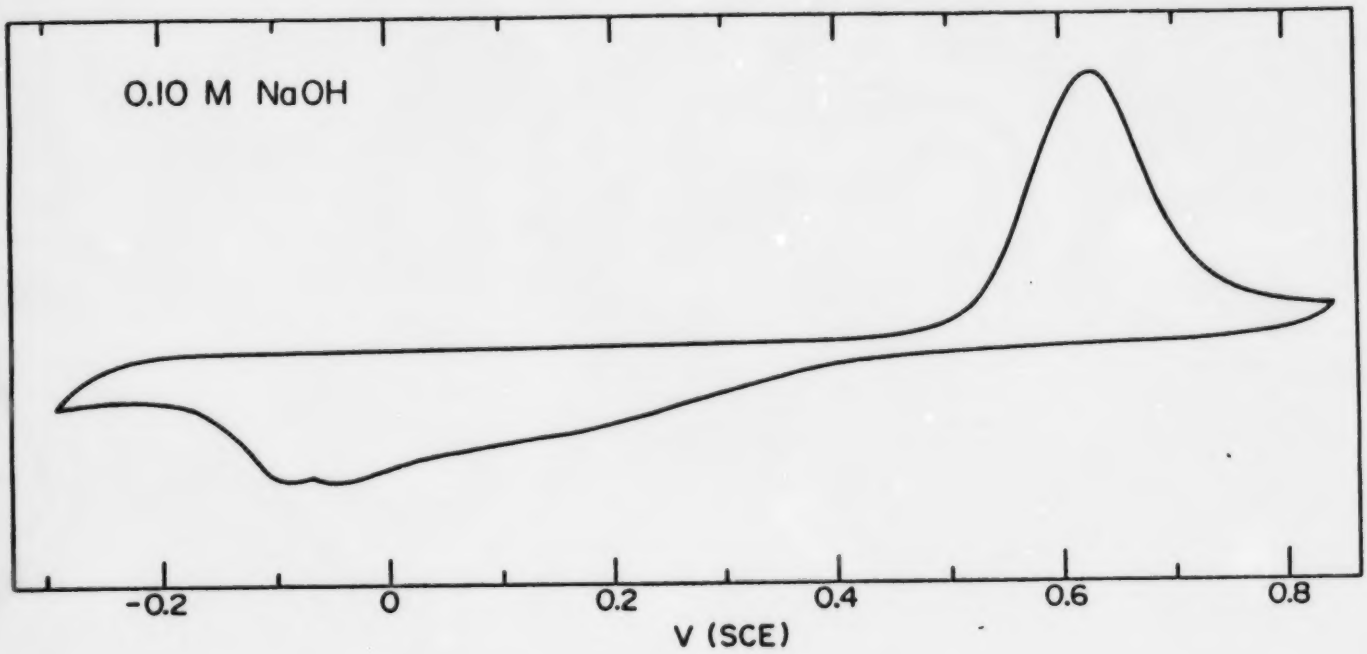


Figure 13: Cyclic voltammogram showing that $Pb^{+2}$ is oxidized to $Pb^{+4}$ at 0.6 V (SCE) while $Pb^{+4}$ is reduced to $Pb^{+2}$ at -0.1 V (SCE).

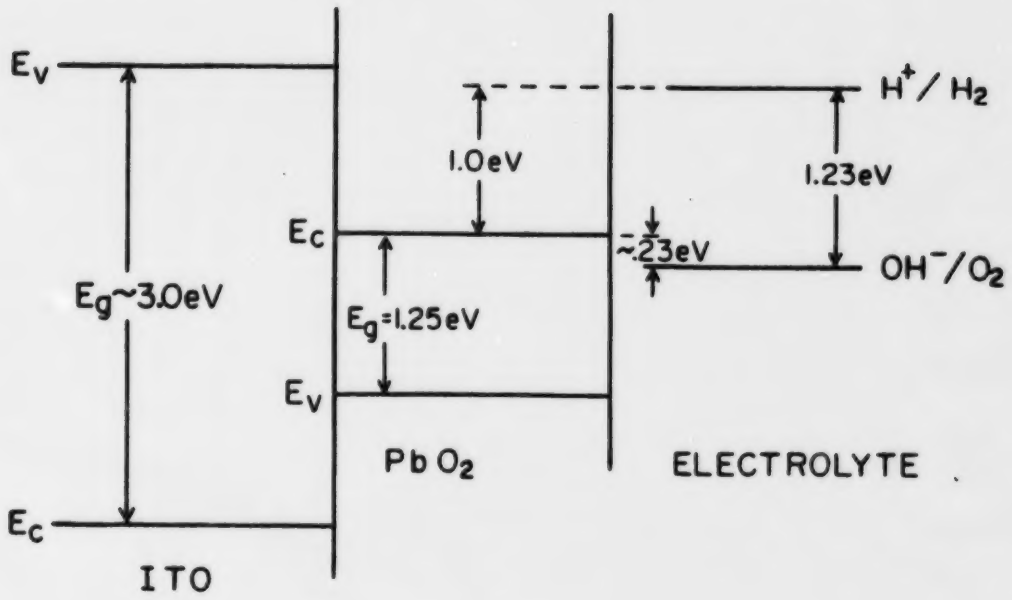


Figure 14: Approximate energy level alignment of the vacuum annealed lead oxide film on ITO, based on experimentally measured $V_{fb}$ and $E_g$.